Electronic Supplementary Material (ESI) for Nanoscale.

Supplementary Information for Parametric study of temperature distribution in plasmon-assisted photocatalysis

Ieng Wai Un,[1*], Yonatan Sivan[1,2]

[1]School of Electrical and Computer Engineering, Ben-Gurion University of the Negev, Israel

[2]Ilse Katz Center for Nanoscale Science and Technology, Ben-Gurion University, Israel

[*]E-mail: iengwai@post.bgu.ac.il

August 7, 2020

S1 Steady state temperature distribution under CW illumination

Under monochromatic CW illumination of low intensity, the difference between the electron and lattice temperatures can be neglected [1, 2], so that the temperature distribution of the system at the steady-state can be obtained by solving the (single temperature) heat equation

$$\begin{cases} \nabla \cdot [\kappa_m \nabla T(\omega, \mathbf{r})] = -p_{\text{abs}}(\omega, \mathbf{r}) & \text{for } \mathbf{r} \text{ in NPs,} \\ \nabla \cdot [\kappa_h \nabla T(\omega, \mathbf{r})] = 0 & \text{for } \mathbf{r} \text{ in the host.} \end{cases} \tag{S1}$$

Here, $p_{\text{abs}}(\omega, \mathbf{r})$ is the absorbed power density, related to the total (local) electric field $\mathbf{E}(\omega, \mathbf{r})$ via $p_{\text{abs}}(\omega, \mathbf{r}) = \frac{\omega \varepsilon_m''(\omega, \mathbf{r})}{2} |\mathbf{E}(\omega, \mathbf{r})|^2$ [3]. This field (thus, the absorbed power density) can be obtained by solving the Maxwell's equations numerically. However, due to the huge number of NPs under illumination, such numerical calculation could be time-consuming or even unfeasible.

The procedure adopted for an approximate calculation of the temperature profile in such samples has been described in detail in [4]. We repeat it briefly here for completeness. Since typically $\lambda, d \gg a$, the particle density is low enough so that the NPs can be considered as optically-independent (i.e., no multiple scattering, see also justification below). In this case, the plasmon-assisted photo-catalyst sample can be effectively approximated by a homogeneous absorbing material such that the local illumination intensity experienced by the NP at $\mathbf{r}_i$ is written as $I(\omega, \mathbf{r}_i) = I_{\text{inc}}(\omega) \exp(-z_i/\delta_{\text{skin}}(\omega))$, where $\delta_{\text{skin}}(\omega)$ is the skin (penetration) depth (equivalently, the inverse of the absorption coefficient) experienced by the incident beam and can be determined by the NP density and absorption cross-section [4],

$$\delta_{\text{skin}}(\omega) = d^3/\sigma_{\text{abs}}(\omega). \tag{S2}$$

For simplicity, the transverse profile of the illumination was also assumed to be uniform within the illuminated area. In addition, since $\kappa_m \gg \kappa_h$, the temperature is uniform within each NP even if $p_{\text{abs}}(\omega, \mathbf{r})$ is highly nonuniform [5, 6]. This allows us to replace the spatial-dependent $p_{\text{abs}}(\omega, \mathbf{r})$ in

each NP by its spatial average, namely, for NP at $\mathbf{r}_i$,

$$\bar{p}_{\mathrm{abs},i}(\omega) = \frac{1}{V_{\mathrm{NP}}} \int_{V_{\mathrm{NP}}} \frac{\omega \varepsilon_m''(\omega, \mathbf{r})}{2} |\mathbf{E}(\omega, \mathbf{r})|^2 d\mathbf{r} = \frac{\sigma_{\mathrm{abs}}(\omega) I(\omega, \mathbf{r}_i)}{V_{\mathrm{NP}}}, \tag{S3}$$

where V_{NP} is the volume of the NP and σ_{abs} is the absorption cross-section of the NP (obtained from Mie theory [7], direct simulations etc.).

In addition, since the heat equation (S1) is a linear differential equation, the temperature rise $\Delta T(\omega, \mathbf{r})$ in the multiple NP problem can be written as the linear combination of all the single NP contributions (denoted by $\Delta T_{(i)}(\omega, \mathbf{r})$) [8], i.e., $\Delta T(\omega, \mathbf{r}) = \sum_i \Delta T_{(i)}(\omega, \mathbf{r})$[1]. Here, the symbol Δ denotes the difference with respective to the temperature in the absence of the illumination (denoted as $T_{h,0}$). Thus, since the temperature rise in the single NP problem is given by [5]

$$\Delta T_{(i)}(\omega, \mathbf{r}) = \frac{V_{\mathrm{NP}} \bar{p}_{\mathrm{abs},i}(\omega)}{4\pi\kappa_h} \begin{cases} 1/a, & \text{for } |\mathbf{r} - \mathbf{r}_i| < a, \\ 1/|\mathbf{r} - \mathbf{r}_i| & \text{for } |\mathbf{r} - \mathbf{r}_i| > a, \end{cases} \tag{S4}$$

then, the temperature rise $\Delta T(\mathbf{r})$ in the multiple NP problem is

$$\Delta T(\omega, \mathbf{r}) = \begin{cases} \dfrac{V_{\mathrm{NP}}}{4\pi\kappa_h} \left[\dfrac{\bar{p}_{\mathrm{abs},i}(\omega)}{a} + \displaystyle\sum_{j \neq i} \frac{\bar{p}_{\mathrm{abs},j}(\omega)}{|\mathbf{r}_j - \mathbf{r}_i|} \right], & \text{for NP at } \mathbf{r}_i, \\ \dfrac{V_{\mathrm{NP}}}{4\pi\kappa_h} \displaystyle\sum_j \frac{\bar{p}_{\mathrm{abs},j}(\omega)}{|\mathbf{r}_j - \mathbf{r}|}, & \text{for } \mathbf{r} \text{ in the host.} \end{cases} \tag{S5}$$

[1]The effective thermal conductivity of the multiple NPs system $\kappa_{h,\mathrm{eff}}$ is, in general, different from that of the single NP system κ_h and is related to the volume fraction of metal $f_m = \dfrac{4\pi a^3}{3d^3}$ in the host by [9–11] $\kappa_{h,\mathrm{eff}} = \kappa_h + \dfrac{3 f_m \kappa_h}{\frac{\kappa_m + 2\kappa_h}{\kappa_m - \kappa_h} - f_m}$ when $f_m < 0.3$. However, since $\kappa_m \gg \kappa_h$ and $f_m \ll 10^{-3}$, we have $\kappa_{h,\mathrm{eff}}/\kappa_h - 1 \ll 10^{-3}$.

S2 An estimate of the steady-state ΔT^{top} under CW illumination

We start with the temperature rise obtained by a summation of the contributions from many other NPs, Eq. (1),

$$\Delta T^{\text{top}} = \frac{I_{\text{inc}}\sigma_{\text{abs}}}{4\pi\kappa_h a} + \sum_{\mathbf{r}'_j \neq \mathbf{0}} \frac{I_{\text{inc}}\sigma_{\text{abs}}}{4\pi\kappa_h} \frac{e^{-z'_j/\delta_{\text{skin}}}}{r_j}. \tag{S6}$$

When the particle number is sufficient large ($> 10^4$), we can approximate the sums by an equivalent integration such that

$$\begin{aligned}\Delta T^{\text{top}} &\to \frac{I_{\text{inc}}\sigma_{\text{abs}}}{4\pi\kappa_h a} + \frac{I_{\text{inc}}\sigma_{\text{abs}}}{4\pi\kappa_h}\frac{1}{d^3}\int_0^H dz' \int_0^{\rho_0} 2\pi\rho' d\rho' \frac{e^{-z'/\delta_{\text{skin}}}}{\sqrt{\rho'^2 + z'^2}} - \frac{I_{\text{inc}}\sigma_{\text{abs}}}{2\sqrt{\pi}\kappa_h d} \\ &\overset{\rho_0 > 10\delta_{\text{skin}}}{\approx} \frac{I_{\text{inc}}\sigma_{\text{abs}}}{4\pi\kappa_h a} + \frac{I_{\text{inc}}}{2\kappa_h}\left(\rho_0 - \delta_{\text{skin}}\right)\left(1 - e^{-H/\delta_{\text{skin}}}\right) - \frac{I_{\text{inc}}\sigma_{\text{abs}}}{2\sqrt{\pi}\kappa_h d}.\end{aligned} \tag{S7}$$

Here, $\rho_0 = \min(\rho_b, D/2)$, such that the integration range includes the illuminated NPs only. The third term in Eq. (S7) is used to cancel the double-counted self-contribution in the second term. Notice that the approximation in the second line of Eq. (S7) is valid when ρ_0 is large enough. For $\rho_0 > 10\delta_{\text{skin}}$, the error is less than 10%. When the NP number is sufficiently large ($> 10^3$), the first and the third terms can be negligible. If $\delta_{\text{skin}} \ll \rho_0$, Eq. (S7) can be further simplified to

$$\Delta T^{\text{top}} \approx \frac{I_{\text{inc}}\rho_0}{2\kappa_h}\left(1 - e^{-H/\delta_{\text{skin}}}\right). \tag{S8}$$

S3 Spatio-temporal evolution of the sample temperature under a pulse train illumination

In order to understand the sample temperature evolution under pulse train illumination and to study its sensitivity to the system parameters, it is instructive to look first at how the sample temperature evolves after a *single pulse* illumination. For convenience, we label the temperature

evolution under a single pulse (multiple pulse) illumination with a subscript sp (mp).

The spatio-temporal evolution of the sample temperature following a single pulse illumination is obtained by [4, 12]

$$\Delta T_{\rm sp}(\mathbf{r},t)=\begin{cases}\Delta T_{{\rm NP},i}(t)+\displaystyle\sum_{j\neq i}\frac{\mathcal{E}_{\rm sp}}{\rho_h c_h}\frac{e^{-z_j/\delta_{\rm skin}}}{(4\pi d_h t)^{3/2}}\exp\left(-\frac{|\mathbf{r}-\mathbf{r}_j|^2}{4d_h t}\right), & \text{for NP at } \mathbf{r}_i\\ \displaystyle\sum_{j}\frac{\mathcal{E}_{\rm sp}}{\rho_h c_h}\frac{e^{-z_j/\delta_{\rm skin}}}{(4\pi d_h t)^{3/2}}\exp\left(-\frac{|\mathbf{r}-\mathbf{r}_j|^2}{4d_h t}\right), & \text{for } \mathbf{r} \text{ in the host,}\end{cases} \tag{S9}$$

where ρ_h is the mass density of the host, c_h is the heat capacity of the host, $d_h \equiv \kappa_h/(\rho_h c_h)$ is the host thermal diffusivity, $\mathcal{E}_{\rm sp} \equiv \langle I_{\rm inc}\rangle \sigma_{\rm abs}/f$ is the energy absorbed per pulse by a NP at the sample surface and $\Delta T_{\rm NP}(t)$ is the temporal evolution of the inner NP temperature [12]. The spatio-temporal evolution (S9) is a result of a series processes. First, the inner temperature of each NP increases due to photon absorption, occurring on a time scale of the pulse duration τ, this time scale is usually very short (a few ps) so that the temporal distribution of the pulse illumination can be described by Dirac delta function, and that the inner temperature rise dynamics is neglected in Eq. (S9). The inner temperature rise of each individual NP depends on its position due to the finite penetration depth of the illumination. For NPs on the sample surface facing the light source, the inner temperature rise is $\mathcal{E}_{\rm sp}/(\rho_m c_m V_{\rm NP}) \approx 0.24$ mK. Next, the inner NP temperature decays due to heat transfer to the host, estimated to occur within $\tau^d_{\rm NP} \equiv a^2\rho_m c_m/3\kappa_h \approx 600$ ps [12]. Most of the absorbed energy leaves the NPs within this process. Then, the sample temperature increases due to the heat diffusion from the (many) other NPs, occurring on a much longer time scale. This heat diffusion keeps the sample warm at from ~ 8 nK to 35 nK for ~ 2 s. Last, the sample temperature decays again to zero when all the thermal energy diffuses out of the sample. Therefore, the spatio-temporal evolution of the sample temperature under the pulse train illumination can be obtained by the linear combination of many solutions of single pulse events, namely,

$$\Delta T_{\rm mp}(\mathbf{r},t)=\sum_{t_k<t}\Delta T_{\rm sp}(\mathbf{r},t-t_k). \tag{S10}$$

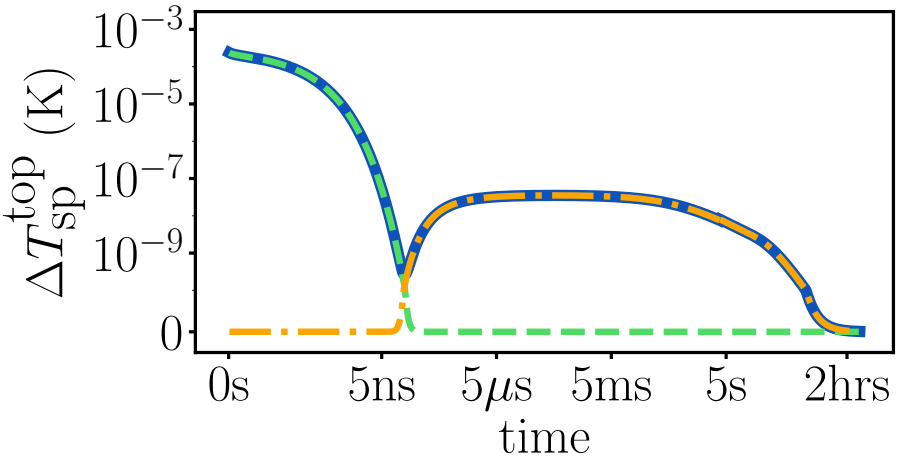

Figure S1: (Color online) (a) The temporal evolution of $\Delta T^{\rm top}$ (blue solid line) following a *single pulse* illumination given by Eq. (S9). The green dash line and the orange dash-dotted line represent the contribution from the inner NP temperature dynamics and from the many other NPs, respectively.

S4 An estimate of the steady-state temperature rise $\Delta T^{\rm top}$ under pulse train illumination

We start with the temporal evolution of $\Delta T^{\rm top}$ under *pulse train* illumination obtained by a summation of many (time-shifted) single pulse events from all particles, Eq. (S9) and (S10), then, we approximate the summation by an equivalent integration, namely,

$$\Delta T_{\rm mp}^{\rm top}(t\to\infty) \to f\int_{1/f}^{\infty} dt' \Delta T_{\rm sp}^{\rm top}(t'), \tag{S11}$$

where

$$\Delta T_{\rm sp}^{\rm top}(t) \to \frac{\mathcal{E}_{\rm sp}}{\rho_h c_h}\cdot\frac{1}{d^3}\int 2\pi\rho' d\rho' dz' \frac{e^{-z'/\delta_{\rm skin}}}{(4\pi d_h t)^{3/2}} \exp\left(-\frac{\rho'^2+z'^2}{4d_h t}\right) \tag{S12}$$

Here, we neglect the contribution from the inner NP temperature dynamics $\Delta T_{\mathrm{NP}}(t)$ in Eq. (S9) since $\tau_{\mathrm{NP}}^{d} \ll 1/f$. The integration over time in Eq. (S11) can be performed analytically, giving

$$\begin{aligned}\Delta T_{\mathrm{mp}}^{\mathrm{top}}(t \to \infty) &= \frac{\mathcal{E}_{\mathrm{sp}} f}{\rho_h c_h} \sum_{\mathbf{r}'_j \neq \mathbf{0}} \frac{e^{-z'_j/\delta_{\mathrm{skin}}}}{4\pi d_h |\mathbf{r}'_j|} \mathrm{erf}\left(\frac{|\mathbf{r}'_j|}{\sqrt{4 d_h t_f}}\right) \\ &= \sum_{\mathbf{r}'_j \neq \mathbf{0}} \frac{\langle I_{\mathrm{inc}} \rangle \sigma_{\mathrm{abs}}}{4\pi \kappa_h} \frac{e^{-z'_j/\delta_{\mathrm{skin}}}}{r'_j} \mathrm{erf}\left(\frac{r'_j}{\sqrt{4 d_h t_f}}\right). \end{aligned} \tag{S13}$$

When $d/\sqrt{4 d_h t_f} > 1.5$, the error function in Eq. (S13) can be replaced by 1, so that Eq. (S13) is reduced to the summation in Eq. (S6). Therefore, $\Delta T_{\mathrm{mp}}^{\mathrm{top}}(t \to \infty)$ can be approximated by

$$\Delta T_{\mathrm{mp}}^{\mathrm{top}}(t \to \infty) \approx \frac{\langle I_{\mathrm{inc}} \rangle \rho_0}{2\kappa_h} \left(1 - e^{-H/\delta_{\mathrm{skin}}}\right). \tag{S14}$$

S5 Simulation results of a catalyst sample in a non-uniform host

In the main text, we study the parametric dependence of the temperature rise based on a simplified model in which the photocatalyst sample has the same thermal conductivity as the outer host. In this section, we aim to verify that the parametric dependence identified by the simplified model are generally applicable to more complicated and realistic systems.

To do that, we first modify our model by replacing the outer host with air so that the catalyst sample and its outer region have different thermal conductivities, as shown in Figure S2(a). We use COMSOL Multiphysics to simulate the temperature distribution and compare them to the results of our model, see Figure S2(b)-(c). This comparison shows that even when the thermal conductivity is non-uniform, the inverse proportionality (see Section 3.1.5) is roughly maintained.

Next, we consider a more realistic configuration which is similar to those used in photocatalysis experiments [13–16]. In this configuration, a disc-shaped catalyst sample (2 cm^2 in surface area and 1 mm in thickness) is loaded on a catalyst bed (2 mm in thickness) and is put in a reaction chamber (2 cm in inner radius and 2 cm in inner height), see Figure S3(a). The catalyst bed has

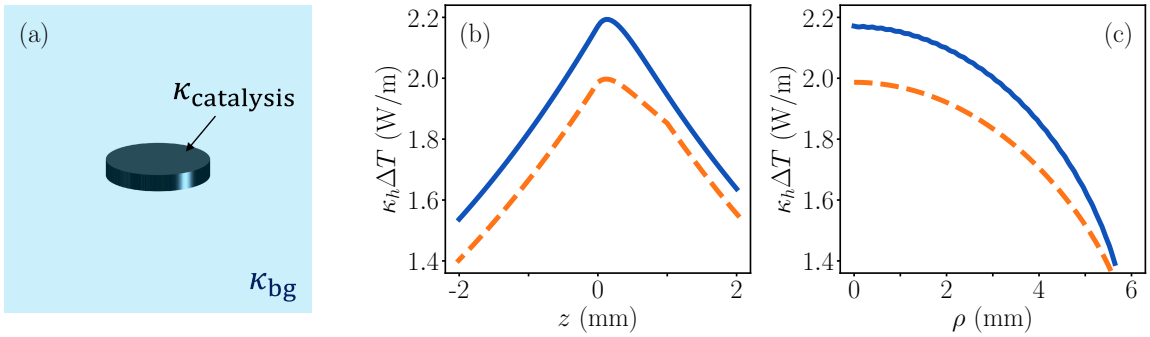

Figure S2: (Color online) (a) Schematic of a disc-shaped catalyst sample immersed in an outer host. (b) $\kappa_h \Delta T$ along the illumination direction and (c) $\kappa_h \Delta T$ along the surface facing the light source. The blue solid lines represent the case in which the catalyst sample and the outer have the same thermal conductivity (homogenized porous oxide), i.e. $\kappa_{\text{catalysis}} = \kappa_{\text{bg}} = \kappa_{\text{porous oxide}}$; ΔT is obtained from Eq. (1) and $\kappa_h = \kappa_{\text{porous oxide}} = 50.3$ mW/(m·K), the same as the blue solid lines shown in Figure 4(a) and (b). The orange dashed lines represent the case in which the catalyst sample has the thermal conductivity of the homogenized porous oxide ($\kappa_{\text{catalysis}} = \kappa_{\text{porous oxide}}$) and the outer is air ($\kappa_{\text{bg}} = \kappa_{\text{air}}$); ΔT is obtained by using COMSOL simulation and $\kappa_h = \kappa_{\text{air}} = 28.8$ mW/(m·K) in this case.

the same thermal conductivity as the catalyst sample. Except for the outer environment of the catalyst sample, all other parameters (the particle size, the inter-particle-spacing, the illumination wavelength, the beam radius and the thermal conductivity of the catalyst sample) are initially taken to be the same as Section 3.1.1. The simulation result of the temperature rise distribution using COMSOL Multiphysics is shown in Figure S3(b). One can see that the maximum temperature rise in the catalyst sample is $\sim$ 36 K, which is $\sim$ 33 K lower than the case in which the catalyst sample is surrounded by air. This is due to the high thermal conductivity of the steel support which is connected to the chamber wall.

In parallel with the results in the main text, we study the parametric dependence of the temperature rise of the configuration shown in Figure S3(a). To do that, as in Section 3, we vary one parameter at a time while keeping all other parameters the same as in Figure S3. Figure S4(a) shows the inter-particle-spacing dependence of the temperature rise at the center of the top surface. When d increases from 100 nm to 225 nm, the NP density decreases by 90% while the overall temperature rise decreases by 2 K ($\sim$ 6%). When d further increases from 225 nm to 300 nm, the NP density decreases by 60% while the overall temperature rise decreases by 5 K ($\sim$ 15%). This shows a fairly weak d-dependence of the overall temperature rise, just like what is shown in Figure 4

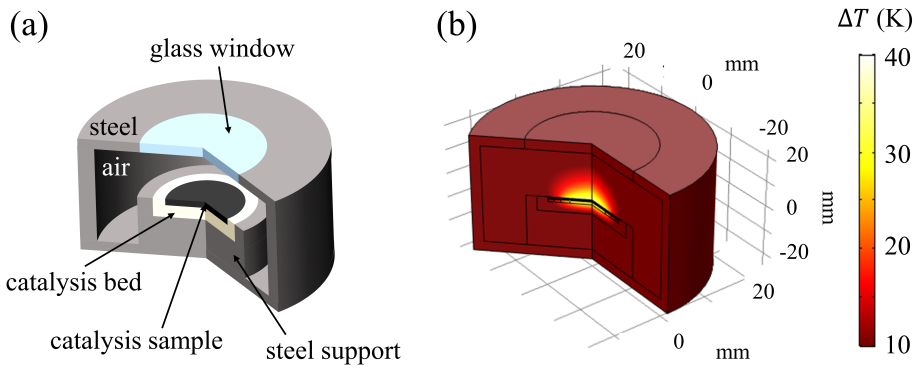

Figure S3: (Color online) (a) A schematic diagram of a disc-shaped catalyst sample put in a steel reaction chamber. The catalyst sample has a surface area of 2 cm^2 and a thickness of 1 mm. The catalysis bed has the same thermal conductivity as the catalysis. All other parameters are the same as in Section 3.1.1 in the main text. (b) The temperature distribution when the catalyst sample is illuminated by a CW laser at the wavelength of 532 nm with a beam area of 1 cm^2.

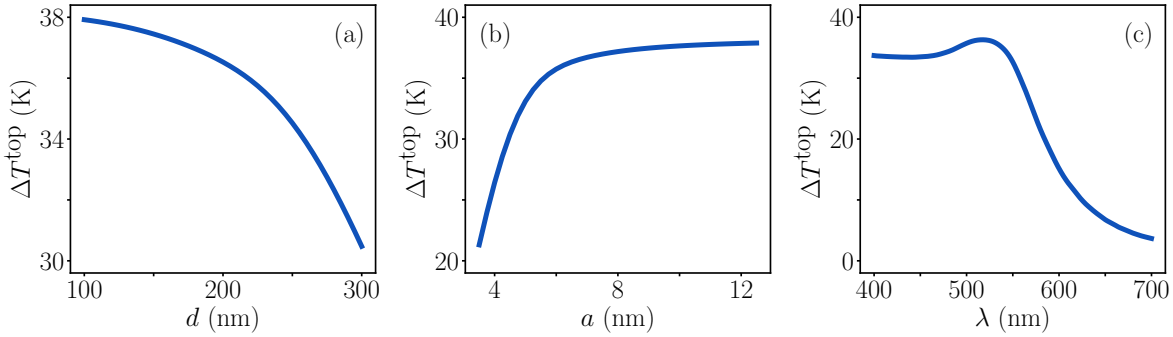

Figure S4: (Color online) (a) The temperature rise at the center of the top surface for different inter-particle spacing. (b) The temperature rise at the center of the top surface for different particle size. (c) The temperature rise at the center of the top surface as a function of the illumination wavelength. In each sub-figure, apart from the parameter of interest, all other parameters are the same as Figure. S3.

in Section 3.1.2. Figure S4(b) shows the particle-size-dependence of the temperature rise at the center of the top surface. As we can see, the temperature rise is weakly dependent on the particle size when $a > 6$ nm. This is similar to what is shown in Figure 5 in Section 3.1.2. Figure S4(c) shows the wavelength-dependence of the temperature rise at the center of the top surface. The ΔT^{top} at the plasmonic resonance wavelength is only 7.7% higher than the short wavelength shoulder. For $\lambda > 580$ nm, the ΔT^{top} becomes roughly proportional to σ_{abs}. The overall weak wavelength-dependence of ΔT^{top} is similar to what is shown in Figure 6 in Section 3.1.3.

Figure S5(b) shows the beam-radius-dependence of ΔT^{top} in log-log scale while the illumination

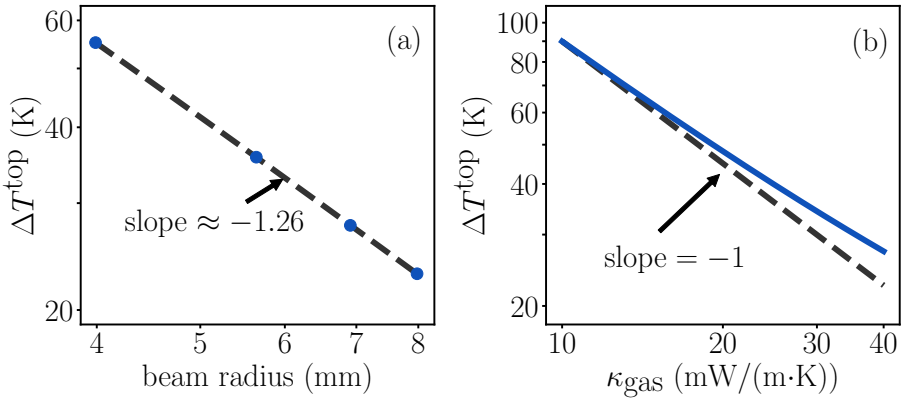

Figure S5: (Color online) (a) The temperature rise at the center of the top surface as as a function of the beam radius in log-log scale (blue dots). The black dashed line is a linear fit to the data (in log-log scale). (b) The temperature rise at the center of the top surface as a function of the gas thermal conductivity in log-log scale (blue solid line). The gray dashed line has a slope of -1 in log-log scale, it represents the inverse proportionality. The ΔT^{top} decreases slightly slower than inverse-linearly with the gas thermal conductivity.

power is fixed. One can see that the ΔT^{top} decreases slightly faster than inverse-linearly with the beam radius, but the inverse proportionality is roughly maintained (slope ≈ -1.26).

Therefore, Figures S2, S4 and S5(a) justify our claim that the qualitative description parametric we identified is not affected by a more realistic configuration accounting of the non-uniformity of thermal conductivity, finite size of the catalyst sample, etc..

Figure S5(b) shows the dependence of the gas-thermal-conductivity-dependence of ΔT^{top} in log-log scale. It shows that the inverse proportionality between ΔT^{top} and κ_{gas} is roughly conserved but ΔT^{top} decreases slightly slower than inverse-linearly with the gas thermal conductivity.

S6 Simulation results of a liquid host

In this section, we study the parametric dependence of the temperature rise of a suspension of Au nanoparticles in a liquid, see Figure S6(a). As we have seen in Section S5, the particle-size-dependence, the inter-particle-dependence and the wavelength-dependence are not affected by the non-uniformity of the thermal conductivity. Therefore, in this section, we will only focus on the dependence of the temperature rise on the thermal conductivity of the liquid. Since the thermal conductivity of liquids is, in general, much larger than that of gas, we use an illumination intensity

of 1 W/cm^2 to achieve a temperature rise of several tens of degrees. Apart from the illumination intensity and the thermal conductivity, all other parameters are the same as Section 3. We initially set the thermal conductivity of the liquid to be 0.6 W/(m·K), corresponding to water. The COMSOL simulation result of the temperature distribution is shown in Figure S6(b). The temperature rise at the illumination spot is around 45 K. Then, we vary the liquid thermal conductivity from 0.4 W/(m·K) to 1.2 W/(m·K) while keep all other parameters to be the same as Figure S6(b). The dependence of the ΔT^{top} on the liquid thermal conductivity (in log-log scale) is shown in Figure S6(c). A linear fit to the data shows that it has a slope of ≈ -0.9. This shows that the inverse proportionality between ΔT^{top} and κ_{liquid} is roughly conserved.

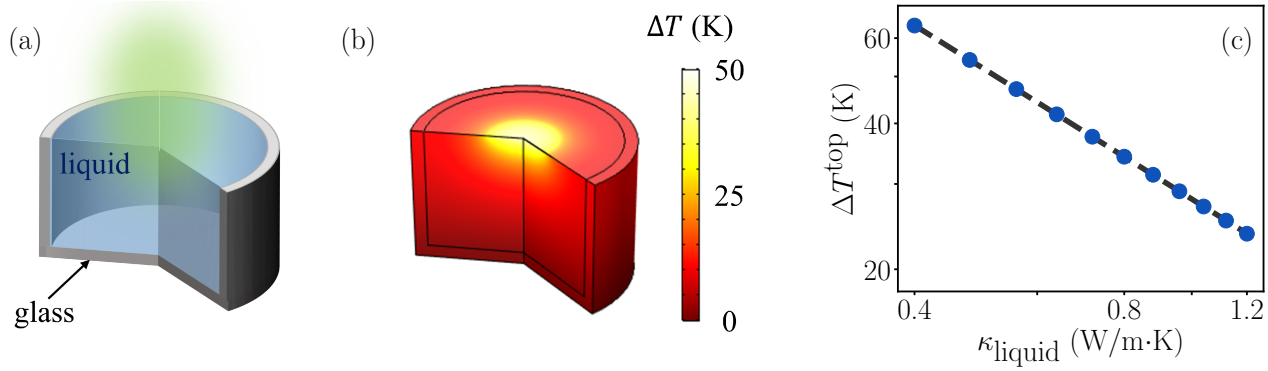

Figure S6: (Color online) (a) A schematic of a suspension of Au nanoparticles in a liquid. A CW laser beam of wavelength 532 nm with beam area of 1 cm^2 is focused at the liquidair interface. (b) The COMSOL simulation result of the temperature distribution. In this case, the thermal conductivity of the liquid is set to be 0.6 W/(m·K) corresponding to water. (c) The ΔT^{top} as a function of the thermal conductivity of the liquid in log-log scale (blue dots). The gray dashed line is a linear fit to the data in the log-log scale. The slope of the linear fit is around -0.9, indicates that the inverse proportionality between ΔT^{top} and κ_{liquid} is roughly conserved.

References

[1] Y. Dubi and Y. Sivan, *Light: Science and Applications: Nature*, 2019, **8**, 89.

[2] L. Meng, R. Yu, M. Qiu and F. J. G. de Abajo, *ACS Nano*, 2019, **11**, 7915–7924.

[3] J. D. Jackson, *Classical electrodynamics*, Wiley & Sons, 3rd edn, 1998.

[4] Y. Dubi, I. W. Un and Y. Sivan, *Chem. Sci.*, 2020, **11**, 5017–5027.

[5] G. Baffou, R. Quidant and F. J. G. de Abajo, *ACS Nano*, 2010, **4**, 709–716.

[6] I. W. Un and Y. Sivan, *J. Appl. Phys.*, 2019, **126**, 173103.

[7] C. F. Bohren and D. R. Huffman, *Absorption and scatering of light by small particles*, Wiley & Sons, 1983.

[8] G. Baffou, P. Berto, E. B. Urena, R. Quidant, S. Monneret, J. Polleux and H. Rigneault, *ACS Nano*, 2013, **7**, 6478–6488.

[9] J. C. Maxwell, *A treatise on electricity and magnetism*, Clarendon Press, 1881, vol. 1.

[10] R. B. Bird, W. E. Stewart and E. N. Lightfoot, *Transport Phenomena 2nd edition,(2002)*.

[11] K. Pietrak and T. S. Wiśniewski, *J. Power Technol.*, 2014, **95**, 14–24.

[12] G. Baffou and H. Rigneault, *Phys. Rev. B*, 2011, **84**, 035415.

[13] S. Mukherjee, F. Libisch, N. Large, O. Neumann, L. V. Brown, J. Cheng, J. B. Lassiter, E. A. Carter, P. Nordlander and N. J. Halas, *Nano Lett.*, 2013, **13**, 240–247.

[14] S. Mukherjee, L. Zhou, A. Goodman, N. Large, C. Ayala-Orozco, Y. Zhang, P. Nordlander and N. J. Halas, *J. Am. Chem. Soc.*, 2014, **136**, 64–67.

[15] L. Zhou, D. F. Swearer, C. Zhang, H. Robatjazi, H. Zhao, L. Henderson, L. Dong, P. Christopher, E. A. Carter, P. Nordlander and N. J. Halas, *Science*, 2018, **362**, 69.

[16] P. Christopher, H. Xin, A. Marimuthu and S. Linic, *Nat. Materials*, 2012, **11**, 1044–1050.